Electrocatalysis

International Edition: DOI: 10.1002/anie.201806298
German Edition: DOI: 10.1002/ange.201806298

Electrocatalytic Oxidation of 5-(Hydroxymethyl)furfural Using High-Surface-Area Nickel Boride

*Stefan Barwe[+], Jonas Weidner[+], Steffen Cychy, Dulce M. Morales, Stefan Dieckhöfer, Dennis Hiltrop, Justus Masa, Martin Muhler, and Wolfgang Schuhmann**

Abstract: *The electrochemical oxidation of the biorefinery product 5-(hydroxymethyl)furfural (HMF) to 2,5-furandicarboxylic acid (FDCA), an important platform chemical for the polymer industry, is receiving increasing interest. FDCA-based polymers such as polyethylene 2,5-furandicarboxylate (PEF) are sustainable candidates for replacing polyethylene terephthalate (PET). Herein, we report the highly efficient electrocatalytic oxidation of HMF to FDCA, using Ni foam modified with high-surface-area nickel boride (Ni_xB) as the electrode. Constant potential electrolysis in combination with HPLC revealed a high faradaic efficiency of close to 100% towards the production of FDCA with a yield of 98.5%. Operando electrochemistry coupled to ATR-IR spectroscopy indicated that HMF is oxidized preferentially via 5-hydroxymethyl-2-furancarboxylic acid rather than via 2,5-diformylfuran, which is in agreement with HPLC results. This study not only reports a low-cost active electrocatalyst material for the electrochemical oxidation of HMF to FDCA, but additionally provides insight into the reaction pathway.*

Upgrading biorefinery products such as 5-(hydroxymethyl)-furfural (HMF) into important industrial feedstock tackles the transition from petroleum-based chemistry towards green and renewable resources. The hydrogenation of HMF leads to the formation of high-energy biofuels such as 2,5-dimethylfuran (DMF),[1] whereas 2,5-furandicarboxylic acid (FDCA), obtained by HMF oxidation, has been reported to be a "green" platform chemical for the chemical industry with the prospect to replace terephthalic acid as a building block for the synthesis of valuable polymers.[2,3] FDCA-based polyethylene 2,5-furandicarboxylate (PEF) is considered to be a renewable alternative for the industrially used polyethylene terephthalate (PET).[1,2] The thermochemical or electrochemical oxidation of HMF is mostly performed under alkaline conditions to provide the necessary hydroxide ions.[4] Thus electrocatalytic HMF oxidation can be coupled with the electrocatalytic hydrogen evolution reaction (HER), leading to an additional product of high economic value, thereby increasing the energy efficiency of the electrochemical HER.[5] HMF can be converted into FDCA in the presence of either homogeneous or heterogeneous catalysts.[6] However, homogeneous catalysis of HMF conversion often suffers from relatively low FDCA yields and poor selectivity. An optimized metal bromide based homogenous catalyst developed already in 1958 provided FDCA yields of 90%, but the separation of FDCA and catalyst recycling remain challenging.[7] On the other hand, heterogeneous catalysts can be separated from the reaction mixture more easily. The high costs of the conventionally employed heterogeneous noble-metal catalysts, such as Pt,[8] Au,[9] Pd,[10] and Ru,[11] warrant efforts to replace them with transition-metal-based catalysts and to find alternative methods for HMF oxidation. In 1990, Grabowski and co-worker reported on the selective electrochemical oxidation of HMF to FDCA in NaOH (1.0 M) using a $Ni(OH)_2$ electrode. However, the yield was only 71%.[12] The comparatively low yield despite high selectivity can be explained by the decomposition of HMF in alkaline solutions.[13,14] At high pH values (>13), HMF degrades into humin-type products, thereby decreasing the effective HMF concentration, which leads to lower than expected product yields. However, HMF oxidation at a Pt electrode at lower pH values (pH 10) generated only trace amounts of FDCA.[13] Evidently, a high working pH value facilitates the selective electrochemical oxidation of HMF to FDCA, but also its degradation.[14] Thus, to increase the product yield, the development of highly active electrocatalysts is of extreme importance. HMF oxidation using Au, Pd, and their alloys supported on carbon black revealed a dependence on catalyst properties, applied potential, and oxidation pathway.[15] However, although noble-metal-based electrocatalysts exhibit a low overpotential for HMF oxidation, they only provide low current densities owing to surface oxidation and surface blocking. Thus large electrode surfaces and high catalyst loadings are required to achieve high reaction rates.[15] Recently, transition-metal-based electrocatalysts, especially compounds or alloys of nickel and cobalt with main-group elements (e.g., P and S) as well as layered double hydroxides (LDHs), were reported to be efficient electrocatalysts for the selective oxidation of HMF to FDCA, achieving high conversions and yields.[14,16] However, recent reports show that NiFe LDHs lack stability during prolonged exposure to highly alkaline electrolyte solutions,[17] while

[*] Dr. S. Barwe,[+] J. Weidner,[+] D. M. Morales, S. Dieckhöfer, Dr. J. Masa, Prof. Dr. W. Schuhmann
Analytical Chemistry—Center for Electrochemical Sciences (CES)
Faculty of Chemistry and Biochemistry
Ruhr-Universität Bochum
Universitätsstraße 150, 44780 Bochum (Germany)
E-mail: wolfgang.schuhmann@rub.de
S. Cychy, D. Hiltrop, Prof. Dr. M. Muhler
Laboratory of Industrial Chemistry
Faculty of Chemistry and Biochemistry
Ruhr-Universität Bochum
Universitätsstraße 150, 44780 Bochum (Germany)
[+] These authors contributed equally to this work.
Supporting information and the ORCID identification number(s) for the author(s) of this article can be found under: https://doi.org/10.1002/anie.201806298.

transition-metal/main-group-element alloys, such as phosphides and borides, form a highly stable core–shell structure, with the initial alloy in the core being protected by a metal hydroxide/oxyhydroxide shell.[18,19] In 2017, we reported on the use of ultrathin high-surface-area nickel boride as a highly active bifunctional HER and oxygen evolution reaction (OER) catalyst.[18] Inspired by promising results for HMF oxidation using metal/non-metal alloys, we employed high-surface-area nickel boride (Ni_xB) as an electrocatalyst to efficiently and selectively oxidize HMF to the prospective platform chemical FDCA in an electrochemical flow-through reactor coupled with downstream analysis of the products by means of high performance liquid chromatography (HPLC). Additionally, we investigated—to the best of our knowledge for the first time—the preferred reaction pathway by operando electrochemistry-coupled attenuated total reflection infrared (EC-ATR-IR) spectroscopy.

High-surface-area Ni_xB was prepared as already reported in detail elsewhere.[18,20] Briefly, Ni_xB was formed by the reduction of nickel chloride with sodium borohydride under oxygen-free conditions and subsequent annealing at 300 °C under argon atmosphere. The product consisted of discrete nanoparticles and very thin sheets, which were X-ray amorphous.[18] An in-depth characterization of the Ni_xB used in this work by X-ray photoelectron spectroscopy, X-ray absorption spectroscopy, X-ray diffraction, high-resolution transmission electron microscopy, atomic force microscopy, and electrochemical water splitting has been reported by Masa and coworkers.[18] The current study focused solely on the electrochemical transformation of HMF into FDCA and its investigation by means of HPLC and operando EC-ATR-IR. Electrochemical HMF oxidation over Ni_xB was performed in an electrochemical flow-through reactor (Figure 1) with a Ni_xB-modified Ni foam (NF) and unmodified NF as anode and cathode, respectively (for further information, see the Supporting Information). Both electrode compartments were separated by a PEEK-reinforced anion exchange membrane. A Hg/HgO reference electrode was placed in the anode compartment to determine the potential. The anode and cathode compartments were fed with 1 M KOH with and without 10 mM HMF, respectively.

SEM images of bare and Ni_xB spray-coated NF show a clear distinction, with small Ni_xB particles clearly visible on the latter (see the Supporting Information, Figure S1). The activity of Ni_xB-modified NF towards HMF oxidation was determined by hydrodynamic linear sweep voltammetry (LSV) at an electrolyte (1 M KOH) flow rate of 18 mL min^{-1} (Figure 1). The electrochemical HMF (10 mM) oxidation achieved a high current density of 100 mA cm^{-2} at a potential of 1.45 V vs. RHE, 170 mV lower than the potential necessary to drive the OER at the same current density (Figure 1). In the absence of HMF, Ni^{2+} to Ni^{3+} oxidation is observed as a pronounced pre-OER peak at 1.44 V vs. RHE. There is a discernible shoulder on the cathodic side of the Ni^{2+} to Ni^{3+} oxidation peak, which reveals that the Ni^{2+} to Ni^{3+} peak is a convolution of the oxidation of Ni from Ni_xB and from the NF support (Figure S2). In the presence of HMF (10 mM), the Ni^{2+} to Ni^{3+} oxidation peak was no longer observed.

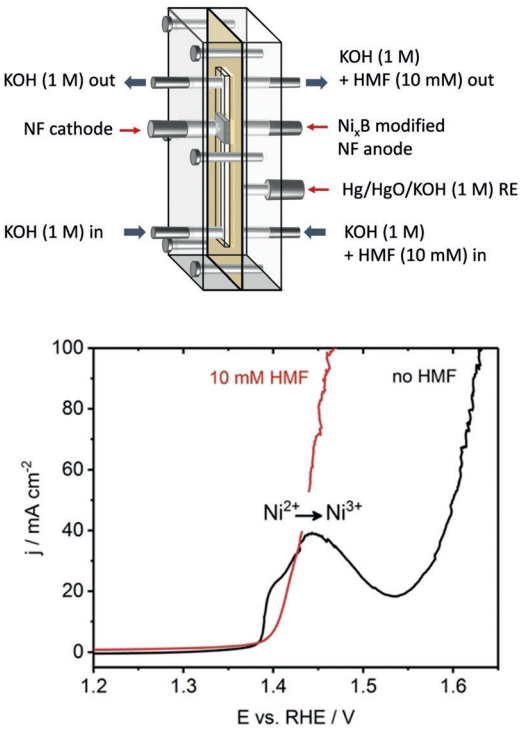

Figure 1. The electrochemical flow reactor (top). LSV of Ni_xB-modified NF in 1 M KOH in the absence and presence of 10 mM HMF with a scan rate of 2 mV s^{-1} at an electrolyte flow rate of 18 mL min^{-1} (bottom).

Interestingly, the more cathodic oxidation feature originating from the NF substrate also disappears in the presence of HMF although HMF oxidation starts at slightly more anodic potentials. Similar observations can be made when bare Ni foam is used for the electrochemical HMF oxidation (Figure S2); in the presence of HMF, the Ni^{2+} to Ni^{3+} peak is not visible anymore although HMF oxidation starts at more anodic potentials. It can be observed that the currents in the presence of HMF rise slowly prior the potential of the $Ni^{2+/3+}$ oxidation recorded in the absence of HMF (Figure S2 b). The absence of the Ni oxidation feature indeed correlates with the presence of HMF and might be overlaid by it. The formation of the higher oxidation state of the transition metal, in this case Ni^{3+}, is a necessary prerequisite for the electrochemical oxidation of alcohols and aldehydes.[21] The presence of HMF altered the electrochemical response, showing an oxidation process at more cathodic potentials as compared to the OER, which is evidently due to electrochemical HMF oxidation. Although the high currents observed by LSV indicate the high activity of Ni_xB towards HMF oxidation, no conclusions about selectivity, reaction pathway, product distribution, and yield can be drawn solely from these data. Downstream analysis is necessary to elucidate the reaction pathways ultimately leading to the products of electrochemical HMF oxidation. Constant potential electrolysis at a potential with apparently negligible OER (1.45 V vs. RHE) coupled with HPLC at different stages of the electrolysis was used to monitor HMF oxidation and the nature of the formed products or intermediates. Oxidation of HMF begins with the oxidation of

either the carbonyl or the hydroxy group to form 5-hydroxymethyl-2-furancarboxylic acid (HMFCA) or the dialdehyde 2,5-diformylfuran (DFF), respectively. Thus the reaction can proceed via two different pathways (Figure 2). Further oxidation of the intermediates HMFCA and DFF

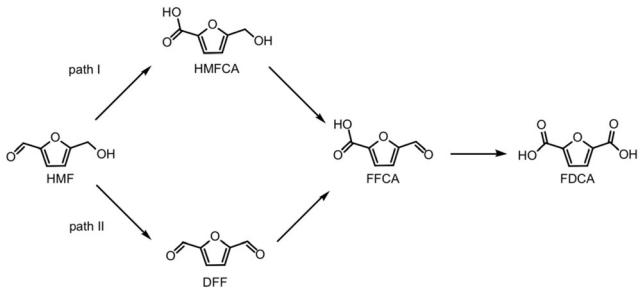

Figure 2. Reaction pathways of HMF oxidation. Pathway I begins with the aldehyde oxidation to form HMFCA. Path II begins with the oxidation of the alcohol group of HMF to give DFF.

leads to the formation of 5-formyl-2-furancarboxylic acid (FFCA) and finally FDCA. Upon applying a constant potential of 1.45 V vs. RHE, the current density instantaneously increased to around 55 mA cm^{-2}. After 2 min, the current density started to decrease, approaching zero after around 35 min (Figure 3a). Correspondingly, the transferred charge showed a steep increase approaching 58.2 C after around 30 min. A charge of 58.2 C for the oxidation of 10 mL 10 mM HMF solution agrees well with the theoretically necessary 6 F mol^{-1} for the complete 6 e$^-$ oxidation of HMF to FDCA, thus indicating that HMF oxidation to the desired product FDCA proceeds with high faradaic efficiency.

HPLC results at different times of the electrolysis qualitatively reveal HMF oxidation to FDCA (Figure 3b; see also the reference chromatograms in Figure S3). The signal attributed to HMF at a retention time of 6.92 min continuously decreased in intensity while that of FDCA at a retention time of 2.88 min increased with time. The intermediate products HMFCA and FFCA were also detected in trace amounts. Interestingly, DFF as a possible intermediate of HMF oxidation was not observed in the chromatograms. Calibration with standard solutions of pure HMF, FDCA, and the intermediates allows for quantification of the compounds during electrolysis (Figure S4). After 10 min of electrolysis, 64% HMF had been converted mainly into FDCA and trace amounts of HMFCA and FFCA as intermediates (Figure 3c). As the intermediates do not accumulate during the process, fast transformation of HMFCA and FFCA into FDCA is suggested. Full HMF conversion was achieved within 30 min with a high FDCA yield of 98.5% and a faradaic efficiency of close to 100% (Figure 3c). The very high yield of 98.5% emphasizes the high activity of Ni_xB towards electrocatalytic HMF oxidation at the applied potential, especially considering a HMF decomposition rate of 10% h^{-1} (for a 10 mM HMF in 1M KOH solution, see Figure S5).

Evidently, using a highly active catalyst for electrochemical HMF oxidation substantially minimizes the extent of the

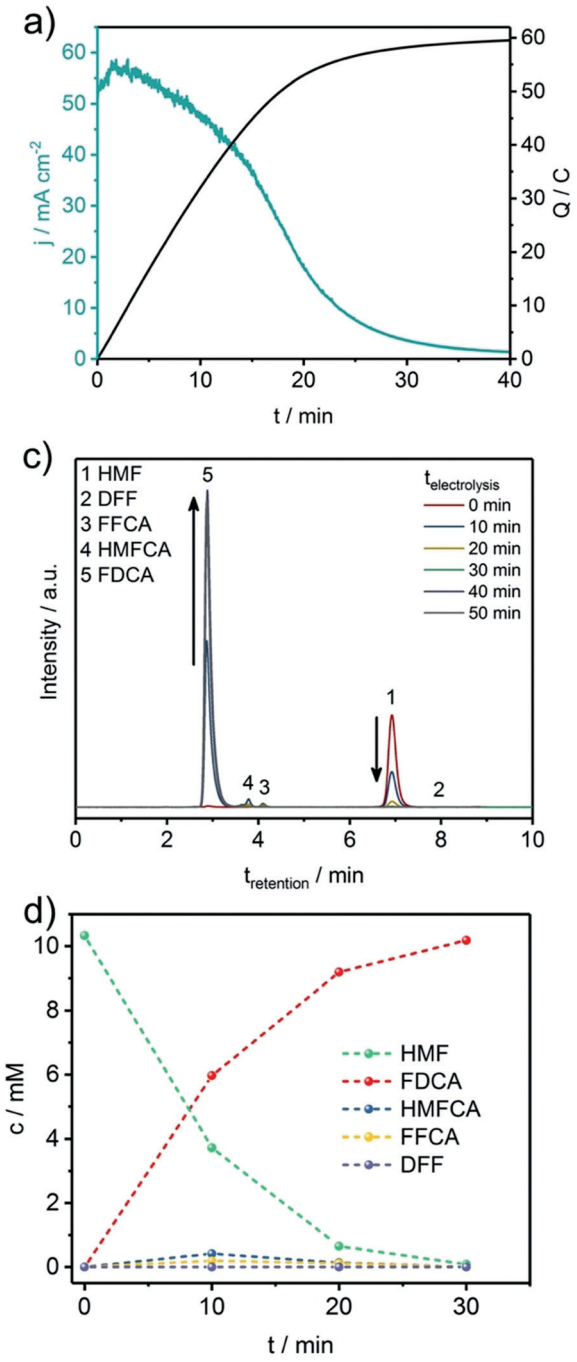

Figure 3. a) Current–time and charge–time transients during constant potential (1.45 V vs. RHE) electrolysis of a 10 mL solution of 10 mM HMF in 1M KOH using a Ni_xB-modified NF anode in a flow reactor with an electrolyte flow rate of 18 mL min^{-1} b) HPLC chromatograms taken at various electrolysis times. c) Concentration versus time plot of HMF, FDCA, and the intermediates at various electrolysis times.

competing chemical degradation of HMF in highly alkaline solution. The used Ni_xB-modified NF was investigated after electrolysis by means of SEM and X-ray photoelectron spectroscopy (XPS). SEM images after electrochemical HMF oxidation (Figure S6) show an intact catalyst film with no obvious changes in the film appearance compared with a freshly prepared electrode. Additionally, freshly prepared

catalyst powder, a fresh Ni_xB-modified NF, and Ni_xB-modified NF after electrochemical HMF oxidation were investigated by XPS (Figure S7). The main binding energy of 852.5 eV in the Ni $2p_{3/2}$ spectrum of the freshly prepared Ni_xB powder is in good agreement with metallic Ni and Ni in contact with B as in Ni_2B (Figure S7 a).[18] Slight surface oxidation upon exposure to air[18] is indicated by the presence of a $Ni(OH)_2$ related peak at binding energies of 855.8 eV (Figure S7 a). Similarly, the B 1s core-level spectrum shows signals originating from elemental B/B-Ni and boron oxo species at binding energies of 187.9 eV and 191.8 eV, respectively (Figure S7 b). After spray-coating and subsequent HMF electrolysis, the Ni $2p_{3/2}$ core-level spectra reveal an oxidized catalyst surface, with $Ni(OH)_2$, NiO, and NiOOH as the main components (Figure S7 c, e). After spray-coating, boron is only present in its oxidized form (B 1s at 192.8 eV) at the catalyst surface (Figure S7 d), while it can barely be detected at the surface after electrolysis (Figure S7 f). Recently, we showed that Ni_xB surface oxidation is also observed upon suspending Ni_xB in a water/ethanol mixture (for spray-coating) and applying anodic potentials.[18] Surface oxidation leads to the formation of a core–shell-type catalyst with oxidized Ni species ($Ni(OH)_2$, NiO, and NiOOH) in the shell and Ni_xB in the core.[18]

To gain further insight into the mechanistic details of the electrochemical oxidation of HMF over Ni_xB, operando EC-ATR-IR spectroscopy was employed. A detailed description of the EC-ATR-IR unit and the micrometer-precise positioning of the working electrode above the ATR crystal was recently reported.[22] LSV under EC-ATR-IR conditions revealed a minor current increase at potentials below 1.45 V vs. RHE and a steep increase in the current response with increasing potential (Figure S8). The early increase in current cannot unambiguously be assigned to HMF oxidation as it might overlay with the Ni^{2+} to Ni^{3+} oxidation. An additional discussion of operando IR can be found in the Supporting Information (Figures S9–S12). The assignment of the IR bands and thus the correlation with the different reaction intermediates was based on comparison with reference spectra (Figure S9) of the pure compounds. The representation of the ATR-IR spectra as the logarithm of the reciprocal reflection leads to downwards and upwards pointing bands for consumed and formed species, respectively. IR spectra recorded during a potential step experiment in the potential range from 0.98 V to 1.78 V vs. RHE not only confirm the oxidation of HMF to FDCA, but also indicate a potential of 1.18 V vs. RHE, at which first IR bands point towards slow HMFCA formation (Figure 4). The bands at wavenumbers of 1386 cm^{-1} and 1351 cm^{-1} and their typical fork-type shape correlate well with the appearance of the HMFCA reference spectrum. At a potential of 1.38 V vs. RHE, the reaction is considerably enhanced, leading to more pronounced HMFCA bands at 1355 cm^{-1}, 1388 cm^{-1}, 1529 cm^{-1}, and 1569 cm^{-1}, while HMF is simultaneously consumed as indicated by the downwards pointing bands at 1027 cm^{-1}, 1189 cm^{-1}, 1513 cm^{-1}, and 1660 cm^{-1}. The fork-shaped band at wavenumbers between 1335 cm^{-1} and 1400 cm^{-1} clearly points to HMFCA as the first detectable intermediate at low potentials. Higher potentials led to further HMF depletion and the appearance of characteristic bands for FFCA and FDCA. The bands at 960 cm^{-1}, 975 cm^{-1}, 1276 cm^{-1}, 1407 cm^{-1}, and 1674 cm^{-1} correlate well with the reference spectrum of FFCA. The very intense peak at 1351 cm^{-1} can neither be unambiguously assigned to FFCA nor to FDCA as both compounds give rise to this band owing to the symmetric vibration of their carboxylate groups. However, FDCA formation is indicated by its characteristic band at 1386 cm^{-1}. Complete conversion of HMF into FDCA cannot be achieved in the thin layer cell of the EC-ATR-IR unit owing to fast reactant depletion in front of the electrode, slow mass transport solely governed by diffusion, and short reaction times. Therefore, the recorded spectra at higher potentials remain convolutions of formed FFCA and FDCA. Nevertheless, complete HMF oxidation into FDCA in the flow reactor was confirmed by HPLC. The possible formation of DFF and its fast oxidation, and thus its absence in the IR spectra and HPLC chromatograms, cannot be ruled out completely. Additionally, the close similarity of the IR spectra of HMF and DFF complicates their clear differentiation. However, IR spectroscopy of DFF and HMFCA in KOH (0.1 M) without applying any potential revealed base-catalyzed oxidation of DFF to FFCA, while HMFCA did not react without an applied potential (Figures S11 and S12). Consequently, whereas the DFF bands might not be clearly assignable, if HMF oxidation preferentially followed reaction pathway II depicted in Figure 2, FFCA-related signals would have to appear in the IR spectra recorded at low potentials without the appearance of HMFCA-related bands. The absence of DFF- and FFCA-related bands at low applied potentials is in good agreement with the HPLC data and strengthens our conclusion that electrocatalytic HMF oxidation on Ni_xB preferentially follows the HMFCA pathway.

In conclusion, we have presented the selective and efficient electrocatalytic oxidation of the biorefinery product HMF to FDCA over Ni_xB-modified NF in an electrochemical

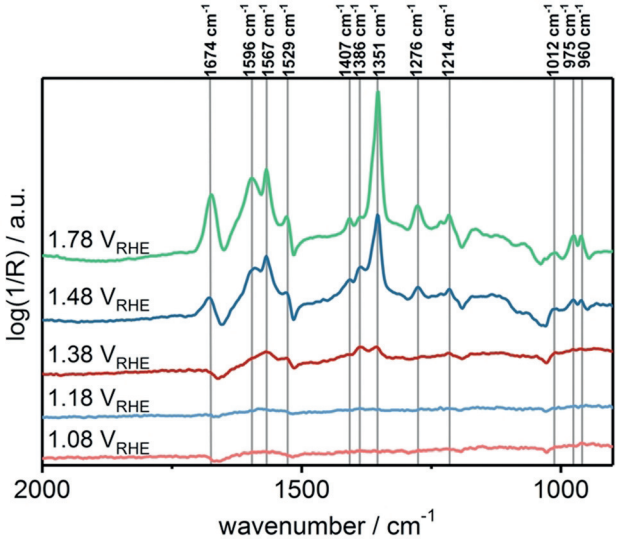

Figure 4. Operando ATR-FTIR spectra recorded at various applied potentials between 0.98 V vs. RHE and 1.78 V vs. RHE after 20 min of applied potential. The potential steps were 100 mV.

flow-through reactor. A very high FDCA yield of 98.5% was achieved at a faradaic efficiency of 100%. The products and intermediates formed were investigated by means of HPLC and operando EC-ATR-IR, revealing that HMF oxidation proceeds via the HMFCA intermediate rather than the DFF pathway. Ni_xB has thus been identified as promising catalyst for electrocatalytic HMF oxidation, an important reaction for upgrading biorefinery products, paving the way towards "green chemistry".

Acknowledgements

This work was supported by the Deutsche Forschungsgemeinschaft (DFG) in the framework of the cluster of excellence RESOLV (EXC 1069) and the CRC/TRR 247 (project A2). We are grateful to Sandra Schmidt for the SEM images and to Dr. Thomas Erichsen and Dr. Dirk Wolters for their help with the HPLC measurements. D. M. Morales acknowledges financial support from Deutscher Akademischer Austauschdienst (DAAD) and Consejo Nacional de Ciencia y Tecnología (CONACyT).

Conflict of interest

The authors declare no conflict of interest.

Keywords: ATR-IR · electrocatalysis · electrosynthesis · HMF oxidation · nickel boride

How to cite: *Angew. Chem. Int. Ed.* **2018**, *57*, 11460–11464
Angew. Chem. **2018**, *130*, 11631–11636

[1] Y. Kwon, K. J. P. Schouten, J. C. van der Waal, E. de Jong, M. T. M. Koper, *ACS Catal.* **2016**, *6*, 6704–6717.
[2] J. J. Bozell, G. R. Petersen, *Green Chem.* **2010**, *12*, 539–554.
[3] a) A. J. J. E. Eerhart, A. P. C. Faaij, M. K. Patel, *Energy Environ. Sci.* **2012**, *5*, 6407–6422; b) R.-J. van Putten, J. C. van der Waal, E. de Jong, C. B. Rasrendra, H. J. Heeres, J. G. de Vries, *Chem. Rev.* **2013**, *113*, 1499–1597.
[4] R. Latsuzbaia et al., *J. Appl. Electrochem.* **2018**, *38*, 4901.
[5] H. G. Cha, K.-S. Choi, *Nat. Chem.* **2015**, *7*, 328–333.
[6] a) T. S. Hansen, I. Sádaba, E. J. García-Suárez, A. Riisager, *Appl. Catal. A* **2013**, *456*, 44–50; b) B. Saha, S. Dutta, M. M. Abu-Omar, *Catal. Sci. Technol.* **2012**, *2*, 79–81.
[7] X. Zuo, P. Venkitasubramanian, D. H. Busch, B. Subramaniam, *ACS Sustainable Chem. Eng.* **2016**, *4*, 3659–3668.
[8] a) H. Ait Rass, N. Essayem, M. Besson, *ChemSusChem* **2015**, *8*, 1206–1217; b) H. Ait Rass, N. Essayem, M. Besson, *Green Chem.* **2013**, *15*, 2240–2251; c) S. Siankevich, G. Savoglidis, Z. Fei, G. Laurenczy, D. T. Alexander, N. Yan, P. J. Dyson, *J. Catal.* **2014**, *315*, 67–74; d) Z. Miao, T. Wu, J. Li, T. Yi, Y. Zhang, X. Yang, *RSC Adv.* **2015**, *5*, 19823–19829; e) S. E. Davis, L. R. Houk, E. C. Tamargo, A. K. Datye, R. J. Davis, *Catal. Today* **2011**, *160*, 55–60.
[9] a) Z. Miao, Y. Zhang, X. Pan, T. Wu, B. Zhang, J. Li, T. Yi, Z. Zhang, X. Yang, *Catal. Sci. Technol.* **2015**, *5*, 1314–1322; b) J. Cai, H. Ma, J. Zhang, Q. Song, Z. Du, Y. Huang, J. Xu, *Chem. Eur. J.* **2013**, *19*, 14215–14223; c) A. Villa, M. Schiavoni, S. Campisi, G. M. Veith, L. Prati, *ChemSusChem* **2013**, *6*, 609–612; d) N. K. Gupta, S. Nishimura, A. Takagaki, K. Ebitani, *Green Chem.* **2011**, *13*, 824–827.
[10] a) B. Liu, Y. Ren, Z. Zhang, *Green Chem.* **2015**, *17*, 1610–1617; b) N. Mei, B. Liu, J. Zheng, K. Lv, D. Tang, Z. Zhang, *Catal. Sci. Technol.* **2015**, *5*, 3194–3202; c) Z. Zhang, J. Zhen, B. Liu, K. Lv, K. Deng, *Green Chem.* **2015**, *17*, 1308–1317.
[11] Z. Zhang, K. Deng, *ACS Catal.* **2015**, *5*, 6529–6544.
[12] G. Grabowski, J. Lewkowski, R. Skowroński, *Electrochim. Acta* **1991**, *36*, 1995.
[13] K. R. Vuyyuru, P. Strasser, *Catal. Today* **2012**, *195*, 144–154.
[14] D.-H. Nam, B. J. Taitt, K.-S. Choi, *ACS Catal.* **2018**, *8*, 1197–1206.
[15] D. J. Chadderdon, L. Xin, J. Qi, Y. Qiu, P. Krishna, K. L. More, W. Li, *Green Chem.* **2014**, *16*, 3778–3786.
[16] a) B. You, X. Liu, N. Jiang, Y. Sun, *J. Am. Chem. Soc.* **2016**, *138*, 6704–6717; b) N. Jiang, B. You, R. Boonstra, I. M. Terrero Rodriguez, Y. Sun, *ACS Energy Lett.* **2016**, *1*, 386–390; c) B. You, N. Jiang, X. Liu, Y. Sun, *Angew. Chem. Int. Ed.* **2016**, *55*, 9913–9917; *Angew. Chem.* **2016**, *128*, 10067–10071; d) W.-J. Liu, L. Dang, Z. Xu, H.-Q. Yu, S. Jin, G. W. Huber, *ACS Catal.* **2018**, *8*, 5533–5541.
[17] C. Andronescu, S. Seisel, P. Wilde, S. Barwe, J. Masa, Y.-T. Chen, E. Ventosa, W. Schuhmann, *Chem. Eur. J.* **2018**, https://doi.org/10.1002/chem.201803165.
[18] J. Masa, I. Sinev, H. Mistry, E. Ventosa, M. de La Mata, J. Arbiol, M. Muhler, B. Roldan Cuenya, W. Schuhmann, *Adv. Energy Mater.* **2017**, *7*, 1700381.
[19] a) J. Masa, S. Barwe, C. Andronescu, I. Sinev, A. Ruff, K. Jayaramulu, K. Elumeeva, B. Konkena, B. Roldan Cuenya, W. Schuhmann, *ACS Energy Lett.* **2016**, *1*, 1192–1198; b) J. Masa, P. Weide, D. Peeters, I. Sinev, W. Xia, Z. Sun, C. Somsen, M. Muhler, W. Schuhmann, *Adv. Energy Mater.* **2016**, *6*, 1502313.
[20] B. Ganem, J. O. Osby, *Chem. Rev.* **1986**, *86*, 763–780.
[21] a) M. Fleischmann, K. Korinek, D. Pletcher, *J. Chem. Soc. Perkin Trans. 2* **1972**, 1396–1403; b) A. Kowal, S. N. Port, R. J. Nichols, *Catal. Today* **1997**, *38*, 483–492.
[22] D. Hiltrop, J. Masa, A. J. R. Botz, A. Lindner, W. Schuhmann, M. Muhler, *Anal. Chem.* **2017**, *89*, 4367–4372.

Manuscript received: May 31, 2018
Revised manuscript received: July 5, 2018
Accepted manuscript online: July 9, 2018
Version of record online: July 31, 2018

